Ultra-high resolution aSNOM imaging at off-resonant wavelengths

Ramazan Sahin[(1),*], Mehmet Günay[(2),*], Alpan Bek[(3)], and Mehmet Emre Tasgin[(2)]
(**1**) *Department of Physics, Akdeniz University, 07058 Antalya, Turkey*
(**2**) *Institute of Nuclear Sciences, Hacettepe University, 06800 Ankara, Turkey*
(**3**) *Department of Physics, Middle East Technical University, 06800 Ankara, Turkey*

An atomic force microscope (AFM) tip, with a few nm-thick noble metal coating, gives rise to strong electric-field at the near-field of tip apex, i.e. hot spot, when illuminated with a beam of light linearly polarized in the axial direction. This strong near-field enables resolving molecular landscape or nano-scale defects on crystal surfaces in apertureless scanning near field optical microscopy or tip enhanced Raman spectroscopy applications. However, strong near fields appear only at certain illumination wavelengths at which material and geometry dependent plasmon resonances take place. Once the metal coated tip is manufactured, optimal operation wavelength remains fixed since the material and geometry of the tip apex remains fixed. Here, we show for the first time a method which renders an AFM tip useful at wavelengths off-resonant to its plasmon resonances. The technique relies on decoration of the tip with appropriate auxiliary molecules. For instance, a tip originally bearing a plasmon resonance at $\lambda_{\rm p} = 581$ nm can be effectively operated off-resonantly at $\lambda_{\rm exc} = 532$ nm, when it is decorated by an appropriate auxiliary molecule. Furthermore, the near-field is found to be strongest just below the auxiliary molecule which enables a single-molecule-size ultra-high spatial resolution imaging. We demonstrate the phenomenon with exact solutions of 3D Maxwell equations. We also show why such an enhancement takes place.

A. Introduction

Metal nano-structures (MNSs) can confine incident radiation into nm-size hot spots thanks to plasmon resonances. This plasmon mediated localization can be 3 to 4 orders of magnitude stronger than the incident field depending on the material, geometry and wavelength [1]. The strong near-field can be utilized for various applications, such as surface enhanced Raman spectroscopy (SERS) and apertureless scanning near field optical microscopy (aSNOM) [2, 3] in which SERS enables the detection of even a single molecule [4] with high spatial resolution [5]. Moreover, increased strength of the nano-scale local near-field at these hot spots also plays a crucial role in achieving high-spatial resolution with sufficient signal-to-noise ratio in aSNOMs which rely on detection of scattered field within the probe-specimen interaction volume. The scattered field generated in the near-field of the probe-specimen interaction is detected at the far-field in various interferometric designs at the specific wavelength of operation. aSNOM produces a 2D spatial map of the near-field that is generated on the surface of the specimen at the operation wavelength.

aSNOM has been used to detect crystallization defects on surfaces [6], to image molecular landscape of biological materials [7], the material distribution of alloys [8], surface phonon polariton waves [9] in a broad wavelength range, etc. Besides the imaging applications, hot spots (generated at the aSNOM tip apexes) can be utilized for nm-size scissors and manipulation purposes, e.g. for manipulating DNA sequences with electromagnetic field [10, 11].

Strong enhancement in the light-matter interaction not only enables the detection of molecules, but it also makes path interference effects appear. When the localized plasmon excitation is coupled to a long-life oscillator, e.g. a dark mode or a molecule, Fano resonances (FRs), referred to as the plasmonic analog of electromagnetically induced transparency (EIT) [12, 13], appear. A transparency window, an absorption dip, shows up in the plasmon spectrum which coincides with the resonance (level-spacing) of the long-life oscillator (molecule) [14].

FRs can control linear response of plasmonic nanostructures. They can do this in two different ways. (*i*) An FR can enhance the lifetime of plasmon excitations near the transparency window [15–18]. This lifetime enhancement leads to a stronger near-field, i.e. dark-hot resonances [19], that is it enhances the linear response. This phenomenon is adopted to enhance the nonlinear processes, such as SERS [20–22] and FWM [23]. Both exciting and converted frequencies are aligned with two FRs.

(*ii*) Alternatively, we demonstrate in this manuscript that, path interference effects can lead to cancellations in the denominator of linear plasmonic response. Coupling to a long-life oscillator (dark mode or molecule) introduces an extra term in the denominator of the excited plasmon amplitude, α, described in full details below Eq. (5) and in Ref. [24]). When a MNS is driven by ($\omega_{\rm exc}$) off-resonantly from its plasmon resonance (Ω), this introduces a nonresonant (Ω-ω_{exc}) term in the denominator. The level spacing of the long-life oscillator, ω_{eg}, can be arranged so that the extra term cancels the nonresonant term (Ω-$\omega_{\rm exc}$). Thus, we show that, a metal nanostructure (MNS) can be operated at an off-resonant frequency, in a 1 nm-width band, as if it is on resonance, or even stronger than the resonance. [1]

[1] Using the same denominator one can also explain why a dip appears at the Fano resonance, i.e. when $\omega_{\rm exc}$=ω_{eg}. Similar cancellation phenomena appear also in nonlinear response [25–27].

In other words, *a plasmon mode can be excited (driven) by a frequency, at which normally no response is expected.* This driven frequency is different than both the plasmon resonance frequency and the resonance frequency of the dark-mode (or QE).

The pronounced phenomenon, off resonance excitation [24] via path-interference, is not to be confused with (*a*) further enhancement of the hot-spot near the transparency (FR) window, i.e. dark-hot resonances [19], and (*b*) off-resonant frequency operation via hybridization. (*a*) Dark-hot resonances take place, owing to the enhanced plasmon lifetime, near the resonance of the long-life oscillation at $\omega_{\rm DM}$ or $\omega_{\rm eg}$. Off-resonance excitation phenomenon takes place at a frequency away from the plasmon resonance Ω and $\omega_{\rm eg}$ (or $\omega_{\rm DM}$). (b) Hybridization (Rabi splitting) [28] yields a shift/splitting of the plasmon (coupled) frequency and possesses a broad band. The path interference effect, we pronounce here, appears only in a window which is smaller than 1 nm spectral width. Second, unlike Refs. [29, 30], we choose the $\omega_{\rm eg}$, Ω and $\omega_{\rm exc}$ non-resonant to each other. That is, even though ω_{eg} is chosen at a frequency where natural band has bi response, path interference still shows up. Third, we observe that this sharp peak is 100 times intenser even than the natural resonance of the MNS, see Fig. 1(b). Fourth, the phenomenon we introduce does not necessitate a strong coupling to exist, provided that choice of a smaller ($\omega_{\rm exc}$-$\omega_{\rm eg}$) can compensate the coupling, see the end of Sec. B.

In this manuscript, we utilize this phenomenon, off-resonant excitation via path interference, to operate a metal coated AFM tip at a very narrow frequency window beyond its plasmon resonances. First, on a basic analytical model we demonstrate how the cancellations in the denominator, of Eq. (5), can give rise to plasmon oscillations at a specific off-resonant frequency. Next, we present the exact solutions of 3D Maxwell equations for a silicon AFM tip with a 10 nm gold coating. We consider an AFM tip decorated scarcely with auxiliary (aux) molecules of resonance $\lambda_{\rm eg}$. We show that a 10^4 times enhanced near-field appears as compared to the incident one (I_0), at $\lambda_{\rm exc}$=532 nm, with an aux molecule of $\lambda_{\rm eg}$=579 nm. The tip originally does not have a plasmon resonance at $\lambda_{\rm exc}$=532 nm. Intensity with the aux molecule is 10^2 times larger even than the near-field at resonances, that is $10^2 I_0$, see Fig. 1(b). Without the aux molecule, the near-field is very close to zero at $\lambda_{\rm exc}$=532 nm. We demonstrate this phenomenon for different aux molecule level spacings, $\lambda_{\rm eg}$'s, where a hybridization is not to be expected, e.g. for $\lambda_{\rm exc}$=473 nm and $\lambda_{\rm eg}$=505 nm in Table I and spectrum Fig. 1(b). Moreover, near the natural resonances, intensity can be increased upto $10^5 I_0$, see Fig. 4, again in a narrow frequency width.

In SNOM, the lateral resolution is limited to about 50 nm, which is the typical size of aperture at the tapered optical fiber end. In aSNOM, since an optical aperture is not required, the lateral resolution can be as low as sub-5 nm, which is determined by the tip apex diameter.

In the proposed technique based on aSNOM, the presence of an aux molecule enhances the field only in a small region below that molecule. Since the $\lambda_{\rm exc}$ is off-resonant to other positions of the tip apex, a striking aux-molecule-size resolution can "in principle" be achieved in aSNOMs, see Figs. 2-4. Finally, we also compare our basic analytical model with 3D simulations. We find that the two results agree with each other for realistic values of the coupling constant. The technique can practically be implemented in a dip-pen nanolithography (DPN) [31], or molecular nanografting-like fashion [32] in an experimental context, where the tip is decorated with molecules by dipping the tip apex deliberately in a droplet of molecule solution (in DPN), or the molecules can be picked from the surface by scratching a dense self-assembled mono-layer occupied area of the sample by the tip (in nanografting). This enables the operation of a manufactured tip at other frequencies than its original plasmonic resonance landscape.

B. A basic analytical model

The system under study consists of a two level QE (aux molecule) with level spacing $\omega_{\rm eg}$ ($\lambda_{\rm eg}$), a conical Au coated AFM tip and an Au substrate. Localized electromagnetic modes, surface plasmon resonances, are supported between the AFM tip and the substrate. The whole system is illuminated with an external field of optical frequency $\omega_{\rm exc}$ ($\lambda_{\rm exc}$). The plasmon field $\hat{a}_{\rm j}$ of the j-th mode produced by the localized surface plasmon excitation is determined by MNPBEM-simulation in the absence of the aux QE, Fig. 1.

The Hamiltonian of the system can be written as the sum of the energy of the plasmon oscillations of the j-th mode ($\Omega_{\rm j}$), quantum emitter ($\omega_{\rm eg}$), the energy transferred by the pump source ($\omega_{\rm exc}$) and the interaction between QE and plasmonic structure

$$\hat{H}_0 = \hbar \sum_{\rm j} \Omega_{\rm j} \hat{a}_{\rm j}^\dagger \hat{a}_{\rm j} + \hbar\omega_{eg} |e\rangle\langle e|, \tag{1}$$

$$\hat{H}_P = i\hbar \sum_{\rm j} (\varepsilon_{\rm j} \hat{a}_{\rm j}^\dagger e^{-i\omega_{\rm exc} t} - {\rm h.c}), \tag{2}$$

$$\hat{H}_{int} = \hbar \sum_{\rm j} f_{\rm j} (\hat{a}_{\rm j}^\dagger |g\rangle\langle e| + \hat{a}_{\rm j} |e\rangle\langle g|). \tag{3}$$

Here $\hat{a}_{\rm j}$ is the annihilation operator of j-th plasmonic mode, $|g\rangle$ ($|e\rangle$) is the ground (excited) state of the QE, $f_{\rm j}$, is the coupling strength between QE and metallic structure in units of frequency. The equations of the motion of the system can be derived by using Heisenberg equations, $i\hbar\dot{\hat{a}} = [\hat{a}, \hat{H}]$. Here we are interested in amplitudes, but not in correlations. We replace the operators $\hat{a}$ and $\hat{\rho}_{mn} = |m\rangle\langle n|$ with complex numbers α and ρ_{mn} respectively [33]. With the addition of damping rates $\gamma_{\rm j}, \gamma_{\rm eg}$ and $\gamma_{\rm ee}$ of j-th plasmon mode, off-diagonal and diagonal elements of QE's density matrix, respectively, we obtain

the following equations for the amplitudes.

$$\dot{\alpha}_{\rm j} = -(i\Omega_{\rm j} + \gamma_{\rm j})\alpha_{\rm j} - if_{\rm j}\rho_{ge} + \varepsilon_{\rm j}e^{-i\omega_{\rm exc}t} \quad (4a)$$

$$\dot{\rho}_{ge} = -(i\omega_{\rm eg} + \gamma_{eg})\rho_{ge} + i\sum_{\rm j} f_{\rm j}\alpha_{\rm j}(\rho_{ee} - \rho_{gg}) \quad (4b)$$

$$\dot{\rho}_{ee} = -\gamma_{ee}\rho_{ee} + i\sum_{\rm j}(f_{\rm j}\rho_{ge}\alpha_{\rm j}^{*} - c.c) \quad (4c)$$

In the steady state, oscillations of the j-th mode of the plasmon amplitude and off-diagonal density matrix element support the driving frequency $\omega_{\rm exc}$ of the form $\alpha_{\rm j} = \tilde{\alpha}_{\rm j}e^{-i\omega_{\rm exc}t}$ and $\rho_{ge} = \tilde{\rho}_{ge}e^{-i\omega_{\rm exc}t}$, respectively. The diagonal density matrix elements do not oscillate in the steady-state, i.e. $\rho_{ii} = \tilde{\rho}_{ii}$ (i=e, g). With addition of the conservation of probability, $\rho_{ee} + \rho_{gg} = 1$, to Eq.(4), one can obtain steady state solution for the plasmon amplitude $\tilde{\alpha}_{\rm j}$ as

$$\tilde{\alpha}_{\rm j} = \frac{\varepsilon_{\rm j} + \sum_{\rm k\neq j}\frac{f_{\rm j}f_{\rm k}^{*}\tilde{\alpha}_{\rm k}y}{i(\omega_{\rm eg}-\omega_{\rm exc})+\gamma_{\rm eg}}}{[i(\Omega_{\rm j}-\omega_{\rm exc})+\gamma_{\rm j}] - \frac{|f_{\rm j}|^2 y}{[i(\omega_{\rm eg}-\omega_{\rm exc})+\gamma_{\rm eg}]}}, \quad (5)$$

where $y = \rho_{ee} - \rho_{gg}$ is the population inversion [34]. A quick examination of the denominator of Eq.(5) can be sufficient to understand the origin of the off-resonant excitation and can be explained as follows. Without the second term in the denominator of Eq. 5, the response is weak when $\omega_{\rm exc}$ is off-resonant to plasmon modes $\Omega_{\rm j}$. However, when the second term is present, the imaginary part of the second term in the denominator of Eq.(5) can be tuned (i.e. by choosing ω_{eg}) to cancel the imaginary part of non-resonant, $i(\Omega_{\rm j}-\omega_{\rm exc})+\gamma_{\rm j}$, term. In practice, this can be done by decorating the Au-coated AFM tip with QEs of appropriate level-spacing. When such a cancellation occurs, the plasmon-QE system can be operated at off-resonance frequencies. One can also consider the other way around. When the AFM-tip is decorated with some molecules, these molecules will yield a resonance out of the actual plasmon resonances, if the ω_{eg} is in a certain (yet not narrow) range.

Moreover, a strong coupling f is not a must for the take place of the cancellation. γ_{eg} is usually very small, $\sim 10^9$-10^{10} Hz, compared to plasmon resonances, $\sim 10^{15}$ Hz. Hence, one can compensate for a relatively small f, by choosing smaller $(\omega_{eg} - \omega_{\rm exc})$ values, in principle.

C. Simulations of 3D Maxwell equations

3D Simulations. We perform simulations with the exact solution of 3D Maxwell equations, in order to test the results of our analytical model, against the retardation effects. We use MNPBEM [35, 36], a freeware boundary element package. In the simulations, the structure is composed of a Au-coated Si AFM tip which is in close proximity of Au substrate. The off-the-shelf AFM tips do not generally have an ultra-sharp end. Therefore, the AFM tip is modeled to be a cone with a round end (radius of curvature of the AFM tip is taken as 50 nm). The tip-sample distance is kept at 5 nm throughout the simulations. Fig. 1 (a) shows the simulated structure. The tip-sample axis is taken to be along the z-axis and the substrate is taken to be in the x-y plane. The illuminating electromagnetic field is taken to propagate in the x-axis with a polarization along the z-axis.

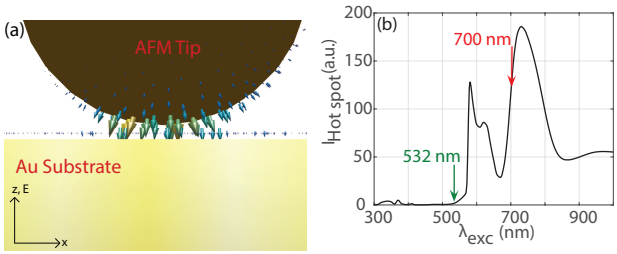

FIG. 1. Exact solutions of 3D Maxwell equations. (a) A Si AFM tip, of radius-of-curvature 50 nm, is coated with 10 nm thick gold. It is positioned 5 nm away from a gold substrate. The system is illuminated with a planewave of polarization along the tip (z-) axis and of wavelength $\lambda_{\rm exc}$ =700 nm. Electric field is localized in the 5 nm gap between the tip apex and the substrate, is indicated with arrows. Simulations are carried out using the freeware software package, MNPBEM [35], which is run using the experimentally determined dielectric functions of Au and Si. (b) The hotspot field intensity. Three plasmon resonances, at $\lambda_{1,2,3}$ =581, 621 and 731 nm appear.

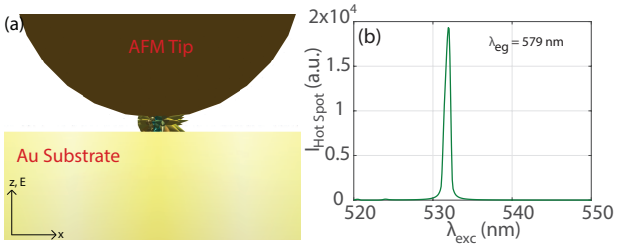

FIG. 2. Demonstration of the off-resonance operation: The field intensity almost vanishes at $\lambda_{\rm exc}$ =532 nm illumination, except for a very small vicinity around the aux molecule. (a) An auxiliary molecule of resonance λ_{eg} =579 nm and diameter 2 nm is placed 1.5 nm below the tip. The setup is illuminated with $\lambda_{\rm exc}$ =532 nm excitation. Molecule is modeled with a Lorenzian dielectric function [37]. (b) A strong electric field of intensity $\sim 2\times 10^4 I_0$ appears around the aux molecule, where path interference takes place. Note that the max hotspot intensity in Fig. 1(b) is only $\sim$200 times of the incident intensity I_0.

When the nano-structure is illuminated with this light source, an intense near-field (hotspot) appears between the AFM tip and the substrate. In order to determine the plasmon resonances, we sweep the excitation wavelength and calculate the hotspot intensity ($I_{\rm HotSpot}$) at each wavelength. Fig. 1(b) shows the $I_{\rm HotSpot}$ values versus the excitation wavelength. Fig. 1(b) shows that the system possesses 3 dominant plasmon modes at 581, 621 and 731 nm [2]. In Fig. 1(a), we plot the hot spot field at the excitation wavelength of 700 nm to show that a strong near-field occurs between the AFM tip and the substrate.

[2] This method cannot determine the dark-modes.

When the setup is illuminated with an excitation wavelength of $\lambda_{\rm exc}$=532 nm, we observe an almost vanishing hot spot intensity, see Fig. 1(b). Next, we position the aux molecule of size 2 nm and λ_{eg} = 579 nm centered at 1.5 nm below the tip apex. We use a Lorentzian dielectric function for the aux molecule [37]. We choose its decay rate as γ_{eg} =2×10^{11} Hz, a moderate quality QE. Our simulations show that, a strong ($10^4 I_0$) electric field localized around the aux molecule appears, where the path interference takes place, see Fig. 2(a). We underline that, excitation wavelength $\lambda_{\rm exc}$ =532 nm is substantially away both from the λ_{eg} =579 nm and from the nearest plasmon mode at λ_1 =581 nm. When we place more of the same aux molecules to random positions on the tip apex we observe a similar behavior (not shown). Electric field is found to be localized around (and below) the aux molecules while it vanishes at nondecorated places. Such a setup can be realized via aforementioned DPL.

To achieve an single-molecule-size resolution, one needs to contaminate the tip with a very diluted solution of appropriate λ_{eg} aux molecules. Still, imaging of a few nm size nanostructure does not necessitate the presence of a single aux molecule at the tip apex. Single-molecule-size ultra-high resolution imaging of such a small sample is possible when the mean spacing between the aux molecules is sufficiently larger than the size of the sample. In Fig. 3, we present a comparison of the $\lambda_{\rm exc}$ =532 nm aSNOM image of a fluorescent nanoparticle of 2 nm diameter (a) without the aux molecule (as in Fig. 1) and with the presence of the aux molecule (as in Fig. 2).

After demonstrating that an AFM tip can be operated at off resonances, we also raise (and answer) the following question. Can we increase the hot spot intensity around (near) the resonances $\lambda_{1,2,3}$? In Fig. 4, we show that using a λ_{eg} = 819 nm aux molecule, the hot spot intensity at the tip apex can be enhanced by a factor of 10^3, above the enhancement value of 10^2, which is attained at a wavelength of $\lambda_{\rm exc}$ = 700 nm within its plasmon resonance band. Use of other λ_{eg} values results in similar enhancement factors for other excitation wavelengths. This appears via cancellations in the denominator of Eq. (5). One can also obtain a spatially uniform enhancement of the tip hot spot, by decorating the the tip apex with more of the same aux molecules. Actually, one can also contaminate the tip with a mixture of different types of aux molecules in order to obtain more number of enhancement peaks, arguably, enabling multicolor aSNOM operation. In Table I, we present the appropriate λ_{eg} values for maximizing the enhancement factor of the hot spot at a variety of widely used laser wavelengths. This setup can also be adapted for high-resolution imaging with a scarce decoration, similar to the one studied in Fig. 2.

$\lambda_{\rm exc}$(nm)	364	378	473	488	532	547	633	688	700
$\lambda_{\rm eg}$(nm)	378	400	505.5	524	579	600	717	800	819

TABLE I. $\lambda_{\rm exc}$(nm) and $\lambda_{\rm eg}$(nm) values for a maximum enhancement of hot spot intensity in the off-resonant excitation.

In Figs. 1-4, we demonstrate the off-resonance operation phenomenon for a hot spot in a tip-Au substrate gap. A demonstration of the same phenomenon for a hot spot at the apex of an AFM tip *without the presence of an Au substrate* is provided in the Supplementary Materials [34].

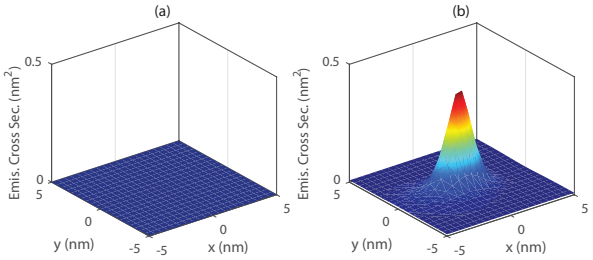

FIG. 3. A high-resolution aSNOM image at λ_{eg} =532 nm of a 2 nm nanoparticle (a) without the auxiliary molecule and (b) with the auxiliary molecule. In (a), we not only obtain an extremely small signal, but the signal almost does not vary within the scanned (±5nm × ±5nm) region, since the radius of curvature of the AFM tip is too large. The nanoparticle is assumed to be a fluorescent dye, which emits at a frequency other than λ_{eg} =532 nm.

D. Comparison with the analytical model

.

We also estimate a coupling parameter, f, by comparing our analytical model with the 3D results. A fit for the damping rates of the 3 plasmon modes, $\lambda_{1,2,3}$ =581, 621 and 731 nm in Fig. 1, yields $\hbar\gamma_{1,2,3}$ = 0.12, 0.16 and 0.22 eV respectively. When we take only the coupling to the closest mode λ_1 = 581 nm, we obtain $\hbar f \simeq 0.19$ eV. This is a typical value close to the estimates of similar studies in the literature [38]. We observe that f is close to the damping rates, which points out an intermediate coupling regime [39, 40]. Actually, independent of the coupling regime, Eq.(5) informs one that off-resonance operation takes place owing to the cancellation of the non-resonant term, $(\omega_{\rm exc} - \Omega_{\rm j})$, in the denominator, whether it is in the strong or weak coupling regime [41, 42]. When we consider coupling to all three modes, we obtain a similar $f_{\rm j}$ value [43].

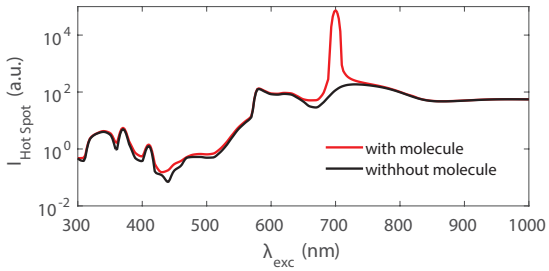

FIG. 4. Hot spot field enhancement near the resonance frequencies: Presence of an aux molecule with $\lambda_{\rm eg}$ = 819 nm can increase the intensity below the molecule to $10^5 I_0$, for $\lambda_{\rm exc}$ =700 nm. This is 3 orders larger than the maximum value obtained at resonance in Fig. 1(b). Phenomenon is not something specific to $\lambda_{\rm exc}$ =700 nm. For other choices of λ_{eg}, similarly, several orders of magnitude enhancement appears at other $\lambda_{\rm exc}$.

E. Summary and Conclusions

In summary, we show that coupling of a long-life oscillator (dark mode or a molecule) can make an AFM tip operate at

a narrow (1 nm) frequency interval which is off-resonant to its natural plasmon bands. Such a phenomenon appears at a certain frequency and a narrow width, where cancelation in the denominator of the plasmon amplitude takse place. This phenomenon appears also when long-life oscillator has resonance e.g. λ_{eg} =505 nm, where plasmon is not excited at all, see Fig. 1(b), distinguishing this work from the existing literature. We also demonstrate, on a single formula Eq.(5), that the phenomenon can appear out of the strong coupling regime. The denominator of this equation explicitly reveals the cancellation effects, unlike the other studies, enhancement of 2-3 orders of magnitude is possible multiplying the intensity at 'resonance' operation.

ACKNOWLEDGMENTS

* These two authors contributed equally. MG and MET acknowledges support from TUBITAK Grant No. 117F118. MET acknowledges support from TÜBA-GEBİP-2017 award.

[1] MI Stockman, "Nanoplasmonics: past, present, and glimpse into future," Optics Express **19**, 22029–22106 (2011).

[2] A Bek, R Vogelgesang, and K Kern, "Apertureless scanning near field optical microscope with sub-10 nm resolution," Review of Scientific Instruments **77**, 043703 (2006).

[3] N Rotenberg and L Kuipers, "Mapping nanoscale light fields," Nature Photonics **8**, 919 (2014).

[4] S Nie and SR Emory, "Probing single molecules and single nanoparticles by surface-enhanced Raman scattering," Science **275**, 1102–1106 (1997).

[5] R Zhang, Y Zhang, ZC Dong, S Jiang, C Zhang, LG Chen, L Zhang, Y Liao, J Aizpurua, Y ea Luo, *et al.*, "Chemical mapping of a single molecule by plasmon-enhanced Raman scattering," Nature **498**, 82–86 (2013).

[6] J Tisler, T Oeckinghaus, RJ Stohr, R Kolesov, R Reuter, F Reinhard, and J Wrachtrup, "Single defect center scanning near-field optical microscopy on graphene," Nano Letters **13**, 3152–3156 (2013).

[7] SG Stanciu, DE Tranca, R Hristu, and GA Stanciu, "Correlative imaging of biological tissues with apertureless scanning near-field optical microscopy and confocal laser scanning microscopy," Biomedical Optics Express **8**, 5374–5383 (2017).

[8] G Kolhatkar, A Boucherif, C Dab, S Fafard, V Aimez, R Arès, and A Ruediger, "Composition variation in al-based dilute nitride alloys using apertureless scanning near-field optical microscopy," Physical Chemistry Chemical Physics **18**, 30546–30553 (2016).

[9] DV Kazantsev and H Ryssel, "Apertureless snom imaging of the surface phonon polariton waves: what do we measure?" Applied Physics A **113**, 27–30 (2013).

[10] M Belkin, S-H Chao, MP Jonsson, C Dekker, and A Aksimentiev, "Plasmonic nanopores for trapping, controlling displacement, and sequencing of DNA," ACS Nano **9**, 10598–10611 (2015).

[11] SJ Heerema and C Dekker, "Graphene nanodevices for DNA sequencing," Nature Nanotechnology **11**, 127 (2016).

[12] N Liu, L Langguth, T Weiss, J Kästel, M Fleischhauer, T Pfau, and H Giessen, "Plasmonic analogue of electromagnetically induced transparency at the Drude damping limit," Nature Materials **8**, 758 (2009).

[13] N Liu, T Weiss, M Mesch, L Langguth, U Eigenthaler, M Hirscher, C Sonnichsen, and H Giessen, "Planar metamaterial analogue of electromagnetically induced transparency for plasmonic sensing," Nano Letters **10**, 1103–1107 (2009).

[14] B Luk'yanchuk, N I Zheludev, SA Maier, NJ Halas, P Nordlander, H Giessen, and CT Chong, "The Fano resonance in plasmonic nanostructures and metamaterials," Nature Materials **9**, 707 (2010).

[15] SM Sadeghi, WJ Wing, and RR Gutha, "Undamped ultrafast pulsation of plasmonic fields via coherent exciton-plasmon coupling." Nanotechnology **26**, 085202 (2015).

[16] ME Tasgin, "Metal nanoparticle plasmons operating within a quantum lifetime," Nanoscale **5**, 8616–8624 (2013).

[17] M ElKabbash, AR. Rashed, B Kucukoz, Q Nguyen, A Karatay, G Yaglioglu, E Ozbay, H Caglayan, and G Strangi, "Ultrafast transient optical loss dynamics in excitonplasmon nano-assemblies," Nanoscale **9**, 6558–6566 (2017).

[18] BC Yildiz Karakul, *Enhancement of plasmonic nonlinear conversion and polarization lifetime via Fano resonances*, Ph.D. thesis, Middle East Technical University (2017).

[19] MI Stockman, "Nanoscience: Dark-hot resonances," Nature **467**, 541–542 (2010).

[20] J Ye, F Wen, H Sobhani, JB Lassiter, P Van Dorpe, P Nordlander, and NJ Halas, "Plasmonic nanoclusters: near field properties of the Fano resonance interrogated with SERS," Nano Letters **12**, 1660–1667 (2012).

[21] Y Zhang, Y-R Zhen, O Neumann, JK. Day, P Nordlander, and NJ. Halas, "Coherent anti-Stokes Raman scattering with single-molecule sensitivity using a plasmonic Fano resonance," Nature Communications **5**, 1–7 (2014).

[22] J He, Cn Fan, P Ding, S Zhu, and E Liang, "Near-field engineering of Fano resonances in a plasmonic assembly for maximizing CARS enhancements," Scientific Reports **6**, 20777 (2016).

[23] Yu Zhang, Fangfang Wen, Yu-Rong Zhen, Peter Nordlander, and Naomi J Halas, "Coherent fano resonances in a plasmonic nanocluster enhance optical four-wave mixing," Proceedings of the National Academy of Sciences **110**, 9215–9219 (2013).

[24] ME Tasgin, A Bek, and S Postaci, *Fano Resonances in Optics and Microwaves: Physics and Application* (Springer Review Book, dated to be published in 2018) Book Chapter 1: "Fano Resonances in the Linear and Nonlinear Plasmonic Response".

[25] SK Singh, MK Abak, and ME Tasgin, "Enhancement of four-wave mixing via interference of multiple plasmonic conversion paths," Physical Review B **93**, 035410 (2016).

[26] BC Yildiz, ME Tasgin, MK Abak, S Coskun, HE Unalan, and A Bek, "Enhanced second harmonic gener-

ation from coupled asymmetric plasmonic metal nanostructures," Journal of Optics **17**, 125005 (2015).
[27] D Turkpence, GB Akguc, A Bek, and ME Tasgin, "Engineering nonlinear response of nanomaterials using Fano resonances," Journal of Optics **16**, 105009 (2014).
[28] Angela Demetriadou, Joachim M. Hamm, Yu Luo, John B. Pendry, Jeremy J. Baumberg, and Ortwin Hess, "Spatiotemporal Dynamics and Control of Strong Coupling in Plasmonic Nanocavities," ACS Photonics **4**, 2410–2418 (2017).
[29] Rohit Chikkaraddy, V. A. Turek, Nuttawut Kongsuwan, Felix Benz, Cloudy Carnegie, Tim van de Goor, Bart de Nijs, Angela Demetriadou, Ortwin Hess, Ulrich F. Keyser, and Jeremy J. Baumberg, "Mapping Nanoscale Hotspots with Single-Molecule Emitters Assembled into Plasmonic Nanocavities Using DNA Origami," Nano Letters **18**, 405–411 (2018).
[30] Nuttawut Kongsuwan, Angela Demetriadou, Rohit Chikkaraddy, Felix Benz, Vladimir A. Turek, Ulrich F. Keyser, Jeremy J. Baumberg, and Ortwin Hess, "Suppressed Quenching and Strong-Coupling of Purcell-Enhanced Single-Molecule Emission in Plasmonic Nanocavities," ACS Photonics **5**, 186–191 (2018).
[31] RD Piner, J Zhu, F Xu, S Hong, and CA Mirkin, "Dip-pen nanolithography," Science **283**, 661–663 (1999).
[32] J Liang and G Scoles, "Nanografting of alkanethiols by tapping mode atomic force microscopy," Langmuir **23**, 6142–6147 (2007).
[33] M Premaratne and MI Stockman, *Adv. Opt. Photon.*, Vol. 9 (2017) pp. 79–128.
[34] See Supplemental Material.
[35] U Hohenester and A Trügler, "MNPBEM–a matlab toolbox for the simulation of plasmonic nanoparticles," Computer Physics Communications **183**, 370–381 (2012).
[36] FJ Garcia De Abajo and A Howie, "Retarded field calculation of electron energy loss in inhomogeneous dielectrics," Physical Review B **65**, 115418 (2002).
[37] X Wu, SK Gray, and M Pelton, "Quantum-dot-induced transparency in a nanoscale plasmonic resonator," Optics Express **18**, 23633–23645 (2010).
[38] MS Tame, KR McEnery, ŞK Özdemir, J Lee, SA Maier, and MS Kim, "Quantum plasmonics," Nature Physics **9**, 329 (2013).
[39] A Delga, J Feist, J Bravo-Abad, and FJ Garcia-Vidal, "Theory of strong coupling between quantum emitters and localized surface plasmons," Journal of Optics **16**, 114018 (2014).
[40] R Thomas, A Thomas, S Pullanchery, L Joseph, SM Somasundaran, RS Swathi, SK Gray, and KG Thomas, "Plexcitons: The role of oscillator strengths and spectral widths in determining strong coupling," ACS Nano **12**, 402–415 (2018).
[41] G Zengin, M Wersäll, S Nilsson, TJ Antosiewicz, M Käll, and T Shegai, "Realizing strong light-matter interactions between single-nanoparticle plasmons and molecular excitons at ambient conditions," Physical Review Letters **114**, 157401 (2015).
[42] P Vasa and C Lienau, "Strong light–matter interaction in quantum emitter/metal hybrid nanostructures," ACS Photonics **5**, 2–23 (2017).
[43] For simplicity, we consider the same value for all f_{j}. We remind that f_j is the overlap integral [24, 44].
[44] M Finazzi and F Ciccacci, "Plasmon-photon interaction in metal nanoparticles: Second-quantization perturbative approach," Physical Review B **86**, 035428 (2012).